ORNL/TM-2015/478

Development and Quality Assessments of Commercial Heat Production of ATF FeCrAl Tubes

Yukinori Yamamoto

September 4, 2015

OAK RIDGE NATIONAL LABORATORY
MANAGED BY UT-BATTELLE FOR THE US DEPARTMENT OF ENERGY

Fuel Cycle Research and Development, Advanced LWR Fuels

Development and Quality Assessments of Commercial Heat Production of ATF FeCrAl Tubes

Yukinori Yamamoto

Oak Ridge National Laboratory

Date Published: September 4, 2015

Work Package Title: ATF Cladding Production
Work Package #: FT-15OR020225
Work Package Manager: Yukinori Yamamoto
Milestone #: M2FT-15OR0202252

Prepared under the direction of the
U.S. Department of Energy
Office of Nuclear Energy
Fuel Cycle Research and Development
Advanced LWR Fuels

Prepared by
OAK RIDGE NATIONAL LABORATORY
Oak Ridge, Tennessee 37831-6285
Managed by
UT-BATTELLE, LLC
for the
U.S. DEPARTMENT OF ENERGY
under contract DE-AC05-00OR22725

This page intentionally left blank

CONTENTS

This page intentionally left blank

LIST OF FIGURES

Page

LIST OF TABLES

Page

This page intentionally left blank

ACKNOWLEDGEMENTS

The author is grateful to Kurt Terrani, Bruce Pint, Lance Snead, Kory Linton, and Mary Snead of Oak Ridge National Laboratory (ORNL) for their helpful discussions, and Tom Geer and Zhiqian Sun of ORNL and Todd Leonhardt, Don Mitchel, Joe Johnson, and Randy Weld of Rhenium Alloys, Inc. for their technical supports. The time spent by Kevin Field and Philip Edmondson of ORNL in reviewing this report is also greatly appreciated.

This research was funded by the U.S. Department of Energy's Office of Nuclear Energy, Advanced Fuel Campaign of the Fuel Cycle R&D program.

This page intentionally left blank

1. ABSTRACT

Development and quality assessment of the 2nd generation ATF FeCrAl tube production with commercial manufacturers were conducted. The manufacturing partners include Sophisticated Alloys, Inc. (SAI), Butler, PA for FeCrAl alloy casting via vacuum induction melting, Oak Ridge National Laboratory (ORNL) for extrusion process to prepare the master bars/tubes to be tube-drawn, and Rhenium Alloys, Inc. (RAI), North Ridgeville, OH, for tube-drawing process. The master bars have also been provided to Los Alamos National Laboratory (LANL) who works with Century Tubes, Inc. (CTI), San Diego, CA, as a parallel tube production effort under the current program.

A warm tube-drawing process was conducted for the initial tube production study with the alloy Fe-13Cr-5.2Al-2Mo-1Nb-0.2Si-0.05Y (designation: C35MN6), although the production was unsuccessful because of a crack formation and propagation, dominantly along the drawing axis. It was found that the premature failure occurred due to several factors; the tube extrusion applied at ORNL produced compressive stress accumulated inside the tube wall, and the stored energy was not fully released because of insufficient annealing process, resulting in non-optimized initial microstructure of the master tubes for conducting the tube drawing process.

The alloys Fe-13Cr-(5.2 or 6 or 7)Al-2Mo-0.2Si-0.05Y (C35M3, C36M2, and C37M, respectively) were used for the second trial, with a careful preparation of the master tubes to avoid any potential issues prior to or during tube drawing process. The tube production of the alloys C36M2 and C37M was suspended after the failure during the drawing pass, which could be due to high work hardenability of the high Al containing alloys. In contrast, optimization of the process parameters for the alloy C35M3 successfully enabled the thin-wall tube production with a size 9.5mm outer diameter and <0.4mm wall thickness. However, there were several quality issues in the thin-wall tube products; such as unexpectedly coarsened grain structure and non-uniform wall thickness. The detailed characterization results and the recommendation of further process optimization have been discussed in the report.

2. INTRODUCTION

The development of nuclear-grade enhanced accident tolerant fuel (ATF) cladding alloys targets a new, metal-base structural material for nuclear fuel cladding, substituting for zirconium-based alloys, that exhibits greatly improved accident tolerance, including good mechanical properties across a wide temperature range as well as oxidation and radiation resistance under normal and transient operating conditions. FeCrAl alloys were selected based on their excellent oxidation resistance in high temperature steam environments up to 1475°C (provided by the sufficient amounts of Cr and Al additions), compared to the industry standard zirconium alloys which do not have such high temperature tolerances [1,2,3,4]. This is the key for enhancing safety margins under severe accident conditions by limiting the heat and hydrogen production, which occurs when the fuel cladding reacts with steam during a severe accident [5]. With superior high temperature strength compared to zirconium alloys, utilization of this class of alloys is expected to enhance burst margins during design basis accident scenarios and potentially for conditions extending beyond those limits.

The deployed design strategy for ATF FeCrAl alloys at Oak Ridge National Laboratory (ORNL) includes improving strength while maintaining high temperature oxidation resistance of FeCrAl alloy(s) resulting in excellent structural and environmental performance under normal operation (~320°C) and potential accident conditions (up to ~1300-1400°C). The ATF FeCrAl alloys should also have good fabricability since the final cladding tube products will need to be fabricated through conventional industrial processing routes (extrusion, drawing, etc.) by commercial manufacturers to keep the ATF cladding option cost effective compared to current Zr-based cladding options. This is one of the important key factors for successful development of the ATF FeCrAl, and the main topic of this milestone report.

The development efforts of ATF FeCrAl alloys were initiated in FY2013 under the Fuel Cycle Research and Development (FCRD) program [6] and consisted of two phases. Phase I was targeted at finding base Fe-Cr-Al-Y alloy compositions of the nuclear-grade FeCrAl alloys for LWR fuel cladding with accident tolerance, through the evaluation of fundamental properties, such as the tensile strength, oxidation resistance, fabricability, and weldability, as a function of the major alloying elements. It was found that the higher Cr addition would be better for corrosion or oxidation resistance to support the stability of alumina-scale in a wide temperature range, although it would increase potential embrittlement of the materials at relatively lower temperatures due to the formation of σ-FeCr or α-Cr phases [7]. Irradiation effects on microstructure evolution, such as accelerated α-Cr formation or the formation of dislocation loops, has been evaluated and discussed under the same program [8]. Weldability of the Phase I alloys was also discussed, and very little effect of the alloy compositions on the weld characteristics was found in the range of 12-17.5 wt.% of Cr and 3-4.4 wt.% of Al [9]. Higher Al additions of up to 7 wt.% was found to be beneficial for the oxidation resistance as well, especially at elevated temperatures [10], but may raise the ductile-brittle transition temperature (DBTT) which could affect the room temperature fabricability [11]. Based on the results in Phase I, a candidate base FeCrAl alloy composition, Fe-13Cr-4.5Al-0.05Y in weight percent, was downselected for further optimization under the second phase of the development program. Variants of the Fe-13Cr-4.5Al-0.05Y are otherwise called "2nd generation ATF FeCrAl alloys"

or “Phase II alloys”. Minor alloying additions were applied through guidance from computational thermodynamics for improved strength together with sufficient oxidation resistance at elevated temperatures, without sacrificing a good fabricability to support FeCrAl thin-wall tube product with commercial manufacturers. The comprehensive summary of the 2nd generation ATF FeCrAl alloy development and property evaluation can be found in the reports previously submitted [12,13,14].

The beneficial effects of minor alloying additions on tensile properties of the Phase I and Phase II alloys are summarized in Figure 1 [13]. It clearly demonstrates that the addition of 2 wt.% Mo improved the yield and ultimate tensile strengths compared to those of the Phase I alloy (T35Y2, Fe-13Cr-4.5Al-Y) due to a solution hardening effect. Further addition of ~1 wt.% Nb resulted in ~25-45% higher yield strengths while maintaining ~10% uniform plastic elongation. The Nb addition played an important role in increasing the thermal stability of the microstructure, and therefore high-temperature mechanical properties, because the dispersion of Fe_2Nb-type Laves-phase precipitates pinned sub-boundary/grain boundary preventing undesirable grain coarsening [12]. It is also illustrated in Figure 1b that the addition of 7 wt.% Al in the Phase I alloy increased both the yield and ultimate strengths similar to the Mo + Nb additions. This seemed a more favorable result since higher Al additions leads to improved oxidation resistance at elevated temperatures [10]. However, there is a concern from the fabricability viewpoint that Al additions increase the work hardenability (the slope after yielding) that would result in increasing deformation resistance. It may reduce the fabricability of the alloys during tube fabrication process, narrowing the window of the process conditions. Therefore, it requires further evaluation of the material characteristics as a function of alloy compositions, in order to realize the ATF FeCrAl tube production.

There are two different approaches to fabricate a seamless thin-wall tube in commercial manufacturers; one is tube-drawing, and the other is pilgering, as shown in Figure 2 [15,16]. The tube-drawing process is widely applied for making thin-wall tubes used in various industries: architectures, boilers, petrochemical and chemical plants, nuclear and fossil energy plants, aerospace, vehicles, medical equipment, appliances, and so on. It requires a die and a mandrel to reduce and control the outer diameter (OD) and the inner diameter (ID) as shown in Figure 2a, and is occasionally conducted under warm conditions (up to ~300ºC, depending on the materials of the die and the mandrel) to make the fabrication process easier. On the other hand, pilgering was developed for manufacturing tubing with ultrathin walls for nuclear fuel cladding in 1950’s [17]. The high-precision tube roller (HPTR) provides a fast, economical way to achieve extreme reductions in diameter and wall thickness. Vertical mass ring (VMR) die is another cold pilgering technology that uses a couple of rotating dies with varying radius for smooth tube deformation to achieve a more than 90% cross-sectional reduction in a single working cycle. Both pilgering approaches can be categorized as compressive production routes similar to a conventional rolling process, and are suitable for applying larger deformation than tube-drawing process, although they typically require a large capital investment and are not feasible for the production of small quantities.

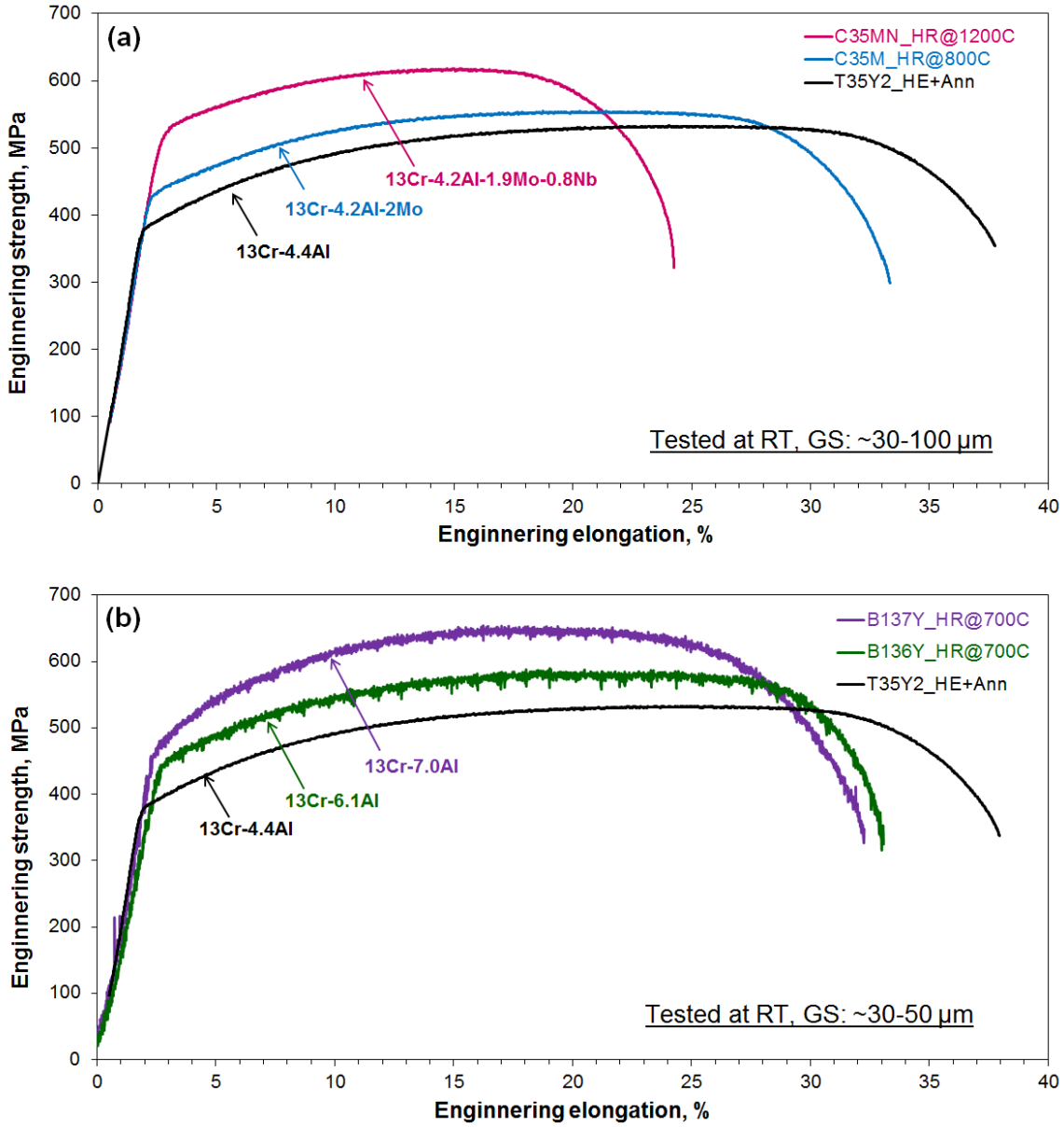

Figure 1. Stress-strain curves of selected Phase I and Phase II alloys tested at RT, showing the effects of (a) the Mo and Nb additions and (b) the Al addition on the tensile properties [13]

The objective of this report is to summarize the recent progress on the 2nd generation ATF FeCrAl cladding development involving commercial fabrication processes, in order to establish the industrial pathway for ATF FeCrAl thin-wall tube production, and to find potential issues that may impact the quality of the final products. A warm tube-drawing process was selected for the initial tube production study because of limited availability of the pilgering equipment in U.S. industry to allow the pilot tube production of new materials of relatively small quantity. The alloy Fe-13Cr-5.2Al-2Mo-1Nb-0.2Si-0.05Y (called as C35MN6) was selected for the first tube production because of the best properties among the developed 2nd generation ATF FeCrAl alloys to date, and the alloys Fe-13Cr-(5.2 or 6 or 7)Al-2Mo-0.2Si-0.05Y (C35M3, C36M2, and

C37M, respectively) were used for the second trial. The alloys with Fe-(10 or 13)Cr-6Al-2Mo-0.2Si-0.05Y (C06M2 and C36M3, respectively) were also prepared and provided to Los Alamos National Laboratory (LANL) for the parallel effort of thin-wall tube production.

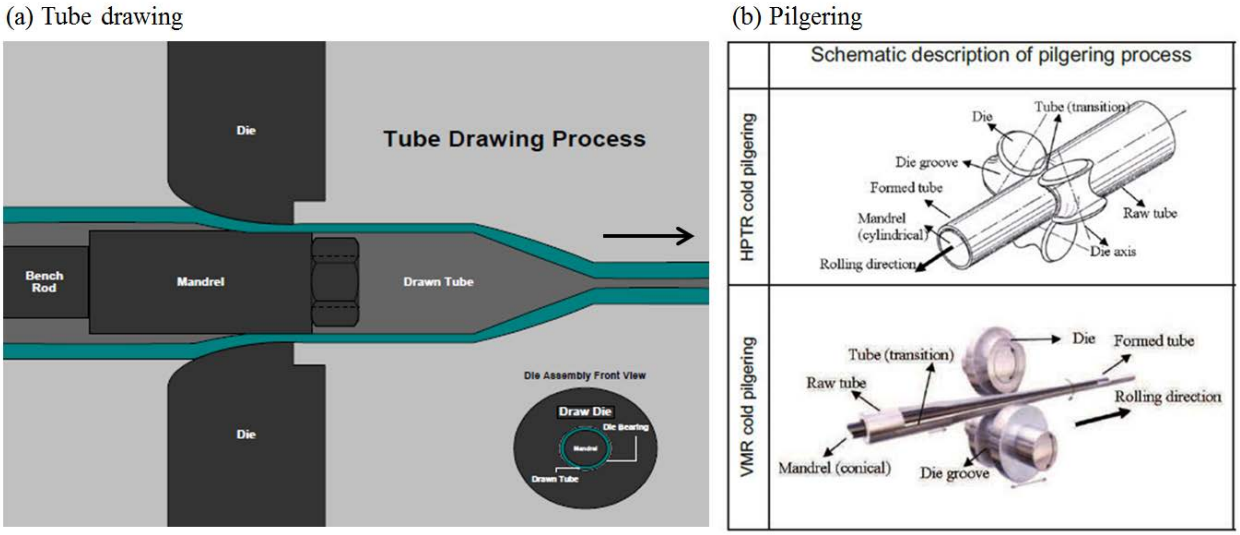

Figure 2. Commercial thin-wall tube fabrication processes; (a) tube drawing with a mandrel [15], and (b) pilgering [16]. Note that HPTR and VMR stand for “high-precision tube roller” and “vertical mass ring die”, respectively

3. MATERIAL PROCUREMENTS

3.1. List of Commercial Vendors

Table 1 summarizes the required processes and the supported commercial manufacturers to conduct the ATF FeCrAl tube-drawing production, including alloy casting, master bar/tube production through extrusion and gun-drilling, and tube-drawing. The cast ingots are provided from Sophisticated Alloys, Inc. (SAI), Butler, PA, who has vacuum induction melt furnaces to produce various alloy ingots up to 500 lbs. The ingots are homogenized and hot-extruded to make them into bar (or tube) shapes and to control the initial microstructure for the subsequent drawing process. The extrusion process with a small quantity has been conducted at ORNL by using the 1250 ton extrusion press. SAI will perform the extrusion process as well once initial feasibility in the tube fabrication process has been demonstrated (planned in FY2016). The extruded bars (or tubes) require a gun-drilling process to make the master tubes to be drawn, which has been conducted by Rhenium Alloys, Inc. (RAI), North Ridgeville, OH. For large quantity production, Grover Gundrilling, LLC, Oxford, ME, will perform the gun-drilling part. The tube drawing process is conducted by RAI who works with ORNL. As a parallel effort of the tube drawing process, LANL is currently working with Century Tubes, Inc., San Diego, CA. Superior Tube Company, Inc. (STC), Collegeville, PA, has a capability of HPTR cold-pilgering, and a discussion of trial pilgering process of the 2nd generation ATF FeCrAl alloys are currently in progress among STC, General Electric (GE), and ORNL.

Table 1. List of commercial manufacturers for thin-wall FeCrAl tube production

Process/product	Manufacturer	Remarks
Cast ingots (>2 lbs.)	Sophisticated Alloys, Inc. (Butler, PA)	Vacuum induction melt, up to 500 lbs.
Hot-extrusion	ORNL	For trial heats, 1250 ton press
	Sophisticated Alloys, Inc. (Butler, PA)	For large quantity production
Gun-drilling	Rhenium Alloys, Inc. (North Ridgeville, OH)	For trial heats
	Grover Gundrilling, LCC (Oxford, ME)	For large quantity production
Tube drawing	Rhenium Alloys, Inc. (North Ridgeville, OH)	Warm-drawing, work with ORNL
	Century Tubes, Inc. (San Diego, CA)	Cold/warm-drawing, work with LANL
Pilgering	Superior Tube Company, Inc. (Collegeville, PA)	Work with GE/ORNL

3.2. Alloy Compositions

Table 2 summarizes the nominal and analyzed compositions of the Phase II alloys to be drawn under the current program. All alloys were prepared by vacuum induction melting through SAI.

Alloy C35MN6 containing nominally 2 wt.% Mo and 1 wt.% Nb was selected for the first trial tube drawing study, and the alloys C35M3, C36M2, and C37M containing various Al contents and 2 wt.% Mo were used for the second trial. The alloys C36M3 and C06M2 were prepared for LANL and GE to conduct the parallel tube drawing efforts and potential pilgering process, respectively. The levels of C, O, N, and S were below 50, 34, 4, and 5 wppm., respectively, which should be low enough to avoid any potential issues to the properties: carbon may form unexpectedly coarsened M_7C_3 or $M_{23}C_6$ type chromium carbides; oxygen and nitrogen may promote internal oxidation and nitridation of aluminum, and sulfur may degrade the stability of protective, external aluminum-oxide layer at elevated temperatures. All alloys were delivered as columnar shape ingots with >3" (75 mm) diameter and >12" (300 mm) length with a hot-top, as summarized in Table 3.

Table 2. Nominal and analyzed alloy compositions (balanced Fe, weight percent)

Sample ID		Cr	Al	Y	Mo	Si	Nb	Remarks
C35MN6	Target	13	5.2	0.05	2	0.2	1	1st trial
	Analyzed	13.00	5.11	0.044	1.99	0.18	0.96	
C35M3	Target	13	5.2	0.05	2	0.2	-	2nd trial
	Analyzed	13.06	5.31	0.053	2.00	0.13	<0.01	
C36M2	Target	13	6	0.05	2	0.2	-	2nd trial
	Analyzed	13.00	6.29	0.059	1.99	0.20	<0.01	
C37M	Target	13	7	0.05	2	0.2	-	2nd trial
	Analyzed	13.01	7.22	0.081	1.99	0.19	<0.01	
C36M3	Target	13	6	0.05	2	0.2	-	For partners
	Analyzed	12.98	6	0.04	1.98	0.18	<0.01	
C06M2	Target	10	6	0.05	2	0.2	-	For partners
	Analyzed	9.88	6.03	0.05	1.97	0.21	<0.01	

Table 3. VIM ingot sizes cast by SAI

ID	Ingot size	Remarks
C35MN6	3.48" (88 mm) diameter x 20" (500mm) length	For ORNL and LANL
C35M3	3.4" (86 mm) diameter x 12" (300 mm) length	For ORNL
C36M2	3.4" (86 mm) diameter x 12" (300 mm) length	For ORNL
C37M	3.4" (86 mm) diameter x 12" (300 mm) length	For ORNL
C36M3	3.2" (81 mm) diameter x 20" (500 mm) length	For LANL and GE
C06M2	3.2" (81 mm) diameter x 20" (500 mm) length	For LANL and GE

3.3. Master Bar/Tube Preparation

All alloy ingots were sectioned into ~6-7" (150-175 mm) length, and then homogenized at 1200ºC for up to 4h in argon cover gas, followed by air-cooling for 5min and then water-quenching. The ingots were then machined into a tube shape or columnar shape to be extruded using a sleeve with a size of 3.5" (89 mm) and 3" (76 mm) diameter, respectively. A mandrel with 0.75" diameter was also used for the tube extrusion. The extrusion was conducted at 1150ºC for two C35MN6 tubes, and at 800ºC for two C35MN6 bars and the rest of alloy bars. The nominal size of the pre- and post-extrusion and the reduction ratio are listed in Table 4. The C35MN6 tubes and the C35M3, C36M2, and C37M bars were sent to RAI in the as-extruded conditions, annealed at 1100ºC (C35MN6 tubes) or 871ºC (the others), straightened at 300ºC, and then gun-drilled and machined to make master tubes to be drawn.

Table 4. Sample size of the material at each step from master tube/bar preparation

ID	Hot-extrusion process			Master tube/bar size
	Pre-extrusion	Post-extrusion	Reduction ratio	
C35MN6	3.3" (84 mm) OD x 1.1" (28 mm) ID	1.325" (34 mm) OD x 0.75" (19 mm) ID	8.1	1.20" (30 mm) OD x 0.80" (20mm) ID
	2.9" (74 mm) dia.	1.125" (29 mm) dia.	6.6	1" (25 mm) dia. x 10" (250 mm) length
C35M3	2.9" (74 mm) dia.	1.125" (29 mm) dia.	6.6	1" (25 mm) OD x 0.80" (20 mm) ID
C36M2	2.9" (74 mm) dia.	1.125" (29 mm) dia.	6.6	1" (25 mm) OD x 0.80" (20 mm) ID
C37M	2.9" (74 mm) dia.	1.125" (29 mm) dia.	6.6	1" (25 mm) OD x 0.80" (20 mm) ID
C36M3	2.9" (74 mm) dia.	1" (25 mm) dia.	8.4	0.9" (23 mm) dia. x 12" (300 mm) length
C06M2	2.9" (74 mm) dia.	1" (25 mm) dia.	8.4	0.9" (23 mm) dia. x 12" (300 mm) length

*OD: outer diameter, ID: inner diameter

3.4. Tube Drawing

Figure 3 shows the apparatus of the tube drawing at RAI. One end of the tube requires to be pointed in order to grab the tube for pulling. The tube will be drawn through the die over a mandrel connected to the bench rod in backward. The tube will be heated up by using a gas burner at the inlet of the die, and the temperature is controlled up to 325ºC in order to minimize the heat impact to the die strength. The detailed die sizes and mandrel sizes in the processes are proprietary, but the area reduction at each pass is in the range from ~9 to ~18%. The drawn tubes are intermediately annealed at various temperatures after 2-3 drawing passes or every pass, depending on the tube conditions. Some of the tubes were sectioned during the drawing process for microstructure characterization by optical microscopes and hardness measurement.

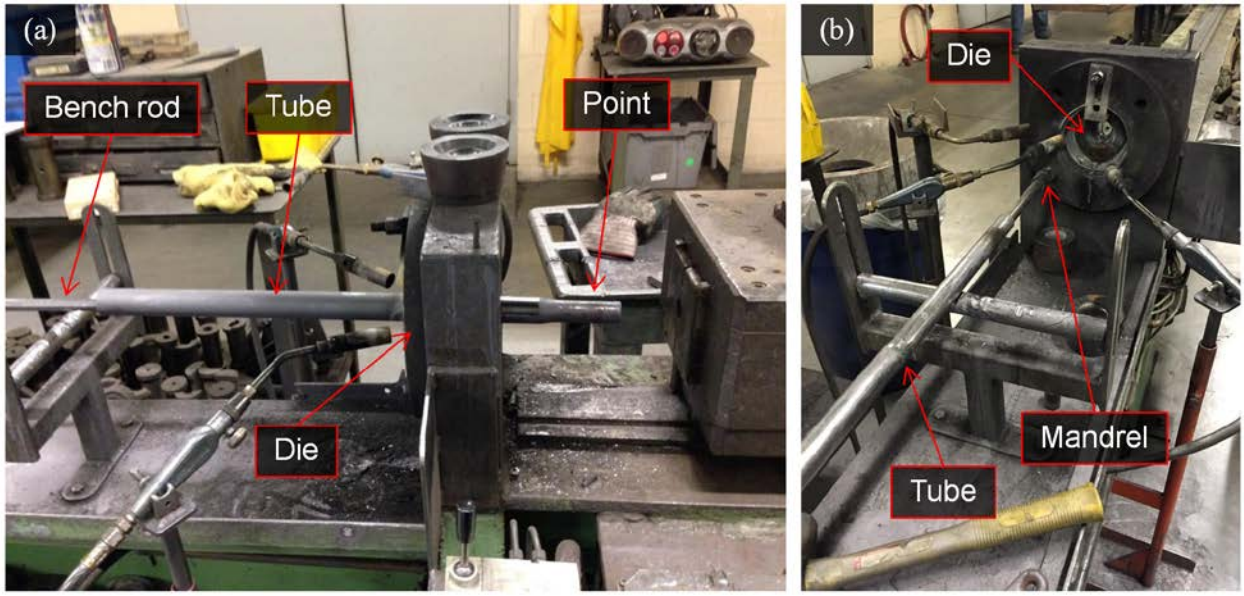

Figure 3. Apparatus of tube drawing at Rhenium Alloys, Inc.; (a) a side view and (b) a rear view.

4. QUALITY EVALUATION

4.1. VIM Ingots and Master Bars/Tubes

In this section, the quality of the ingot and master bars/tubes will be discussed. Since the analyzed compositions of the ingots have been shown in Table 2 and levels of impurities discussed, the quality evaluation of the cast ingot focused on the castability and solidification defects. The quality of the master tubes/bars has also been discussed based on the cross-sectional microstructure observation.

4.1.1. C35MN6

Figure 4 shows pictures of the as-received VIM ingots of the alloy C35MN6. The ingot consists of a main body with ~20" (~500mm) length and a hot-top to prevent the solidification shrinkage inside the main body. Most of the main body area showed no external defects on the surface, although there are cracks near the hot-top, perpendicular to the columnar axis, as shown in Figure 4b. This was due to a tensile stress during the solidification process. The positions of both the hot-top and most of the main body were rigid because of the hot-top shape and the wall friction, respectively, so that the tensile stress would be accumulated at the "neck" position just below the hot-top. The ingots were sectioned just below the cracks. The cross-section of the ingot near the hot-top is shown in Figure 4c, which indicates that hair cracks appeared at the center of the ingots. Although detailed characterization has not been conducted yet, they seem like hot-cracks since the cracks were observed at the solidification ends. Such hair cracks were not observed within the sectioned main body, so it was assumed that these hot-cracks would occur only near the hot-top or they would be a closed defect which could be eliminated by extrusion process.

The main body were sectioned into small pieces with ~6-7" (~150-175 mm) length, homogenized at 1200ºC, and then machined into a billet with cleaned surface to be extruded, as shown in Figure 5. Figure 6a shows the ingots with a center hole that was prepared for tube extrusion with a mandrel. Figure 6b illustrates the as-extruded tubes. Unfortunately, there was a crack formed at the edge of the tube, as shown in the cross-sectional picture, so that the tube was sectioned repeatedly until no crack would be observed. The extruded tubes were then sent to RAI, and machined into master tubes to be drawn, as shown in Figure 6c. One of the master tubes still showed the cracks along the longitudinal axis, but most of the master tubes appeared to have no further defects. It should be noted that the C35MN6 extruded bars were also fabricated at ORNL, and then a part of the bars were provided to LANL for the parallel tube drawing study.

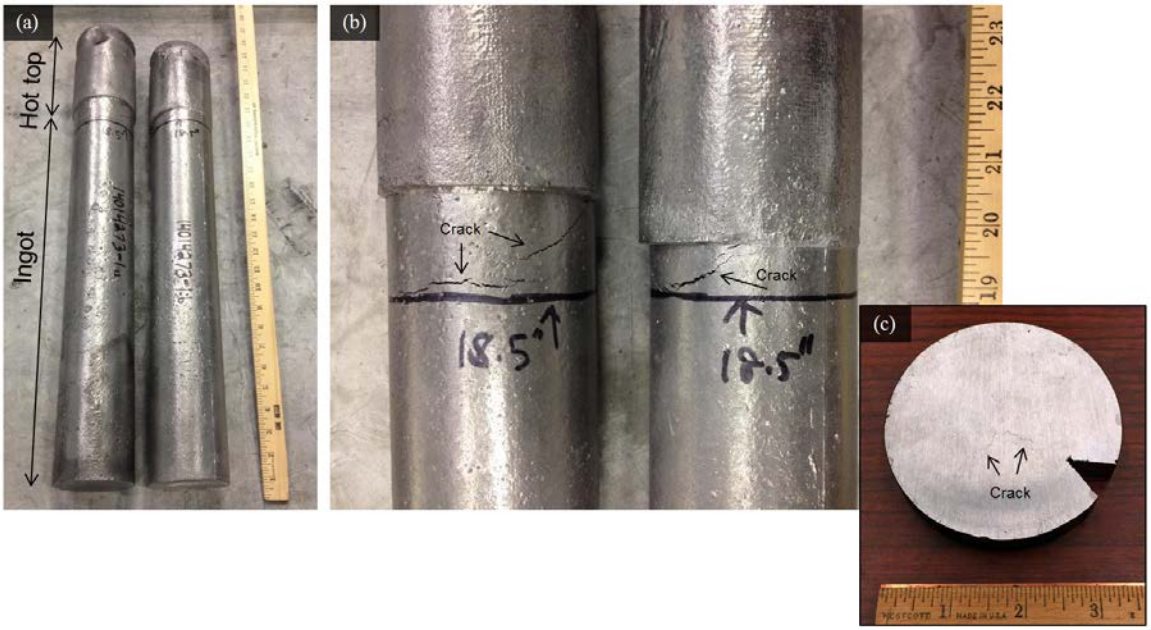

Figure 4. VIM ingots of C35MN6 (Fe-13Cr-5.2Al-2Mo-1Nb alloy) cast by Sophisticated Alloys, Inc.; (a) as-received ingots, (b) a cross-view near the hot-top showing external cracks, and (c) the cross-section near the hot-top also showing internal cracks

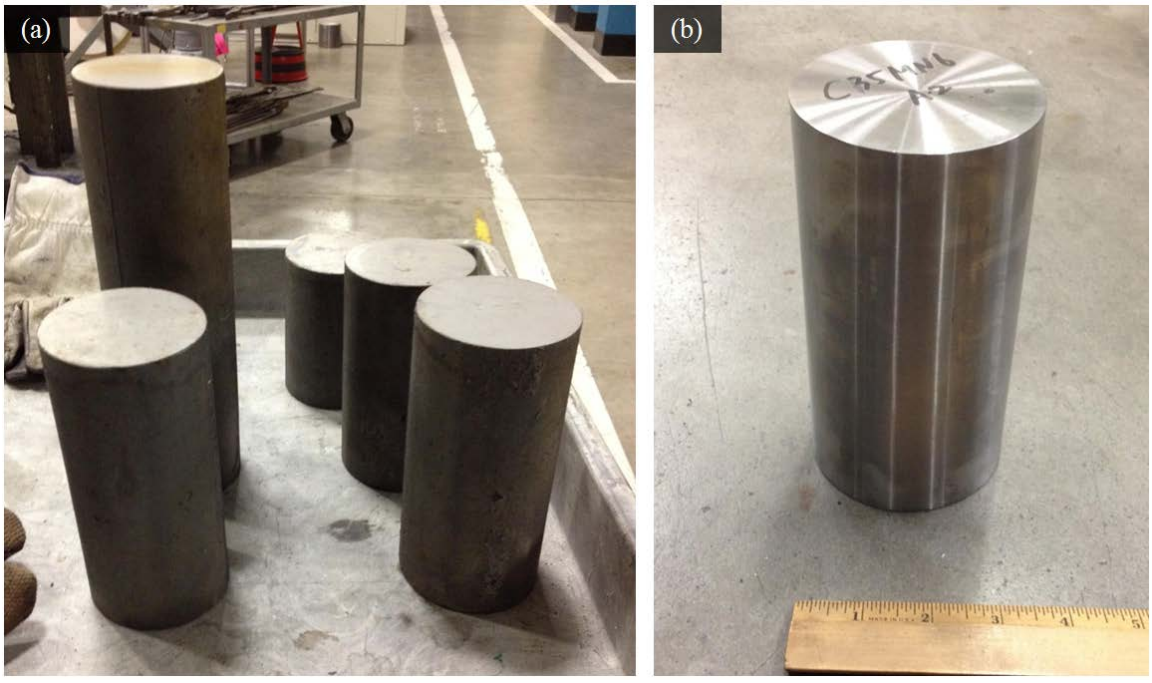

Figure 5. C35MN6 ingots; (a) after sectioning and homogenization, and (b) after machining

Figure 7 shows the cross-sectional micrographs of the as-extruded tubes. The longitudinal section indicates the aligned, elongated grain structure along the extrusion axis, and they seem uniform macroscopically. On the other hand, the transverse section shows inhomogeneous grain structures with relatively coarse grains (bright contrast) dispersed “uniformly”, and there is a

crack starting from the internal surface of the tube. Transgranular cracks propagate through non-recrystallized, coarse grains, with an angle of nearly 45º to the radial axis. There is no severe oxidation along the crack, indicating that the crack formed after the homogenization process or during the extrusion process. These results indicate that a huge compressive stress has been accumulated at the inner surface of the tube, along the circumference. It can easily be speculated that such stored energy also remains in the tubes even without visible cracks.

Figure 8 shows optical micrographs of the C35MN6 tube in the as-extruded condition and after annealing at 1100ºC for 10min. The as-extruded microstructure consists of the elongated grains originating from the cast structure, together with dynamically recrystallized grains with the size of <~100μm aligned along the extrusion direction. On the other hand, the annealed microstructure exhibits fully recrystallized grain structure with ~200-500μm size, indicating that all stored energy during the extrusion process has been released. Based on these results, the same annealing condition (1100ºC for 10 min) is suggested to RAI prior to the drawing process.

Figure 6. C35MN6 samples; (a) after machining with a center hole, (b) after tube-extrusion with a mandrel, and (c) after straightening and surface grinding

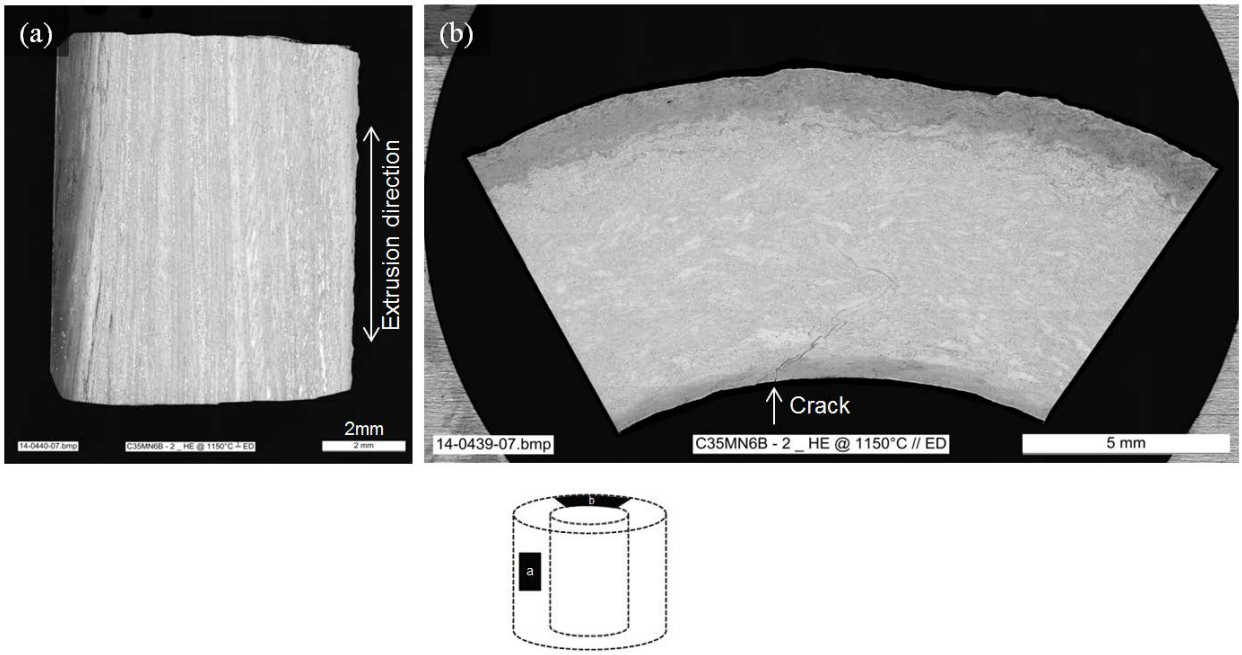

Figure 7. Montage of the cross-sectional micrographs showing as-extruded macrostructure of C35MN6; (a) longitudinal section, and (b) transverse section

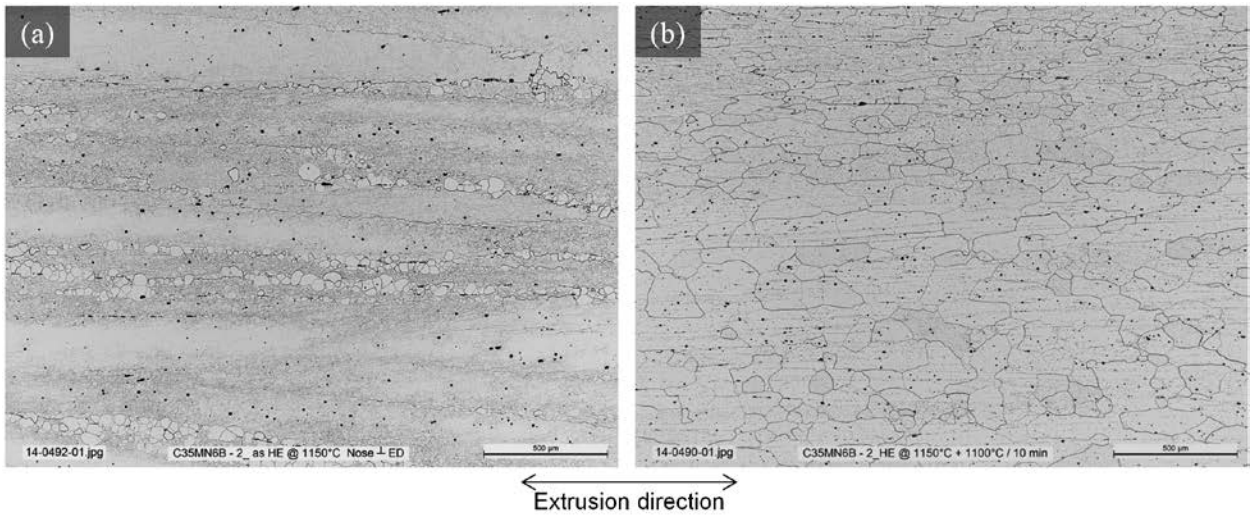

Figure 8. Optical micrographs showing microstructure of extruded C35MN6; (a) as extruded, and (b) after annealing at 1100ºC for 10min

4.1.2. C35M3/C36M2/C37M

VIM ingots of the alloys C35M3, C36M2 and C37M are shown in Figure 9. The main body lengths of the ingots were ~12” (~300 mm). The hot-top remained only on the C35M3 ingot, but there was no apparent crack at the “neck” below the hot-top. This indicates that the shorter main body would help to avoid the defect formation as can be easily imagined. No other external

defects were observed in any of the as-received ingots. They were sectioned into ~6” (~150 mm) lengths, homogenized, machined, and then extruded at 800ºC into bar samples as shown in Figure 10a. They were annealed at 800ºC, and then sent to RAI for straightening and gun-drilling to make the master tubes as shown in Figure 10b. No cracks were observed in the master tubes.

The extruded and annealed microstructures of the alloys are shown in Figure 11. They showed fully recrystallized grain structure with the grain size of ~30-80 μm range, which was consistent with the previous report [12]. They also showed dark-contrast particles aligned along the extrusion direction, which corresponds to yttrium-rich oxides formed along the grain boundary of the original cast structure [13] and still remained after extrusion and annealing processes. Since the grain structures showed no significant difference among the alloys, the material characteristics to be obtained later should be attributed to the Al contents.

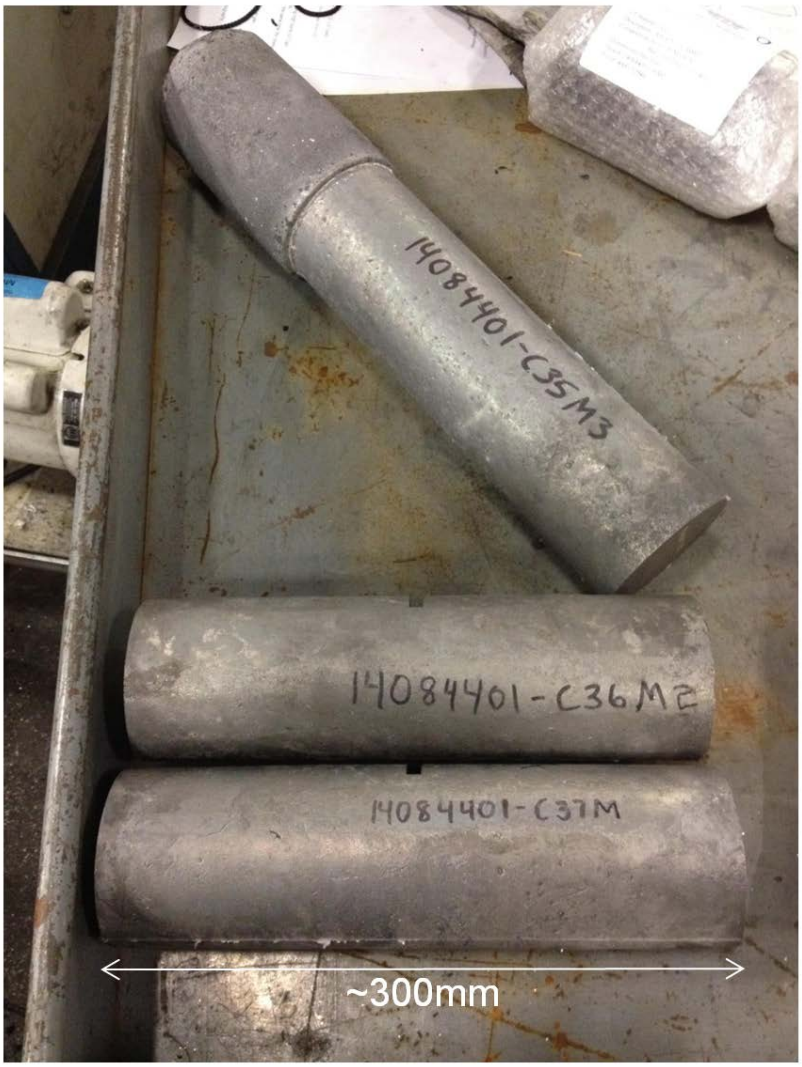

Figure 9. VIM ingots of C35M3, C36M2, and C37M (5.2Al, 6Al, and 7Al containing alloys, respectively) cast by Sophisticated Alloys, Inc.

Figure 10. C35M3, C36M2, and C37M extruded bars and master tubes to be tube-drawn; (a) extruded master bars, and (c) master tubes after gun-drilling and surface grinding

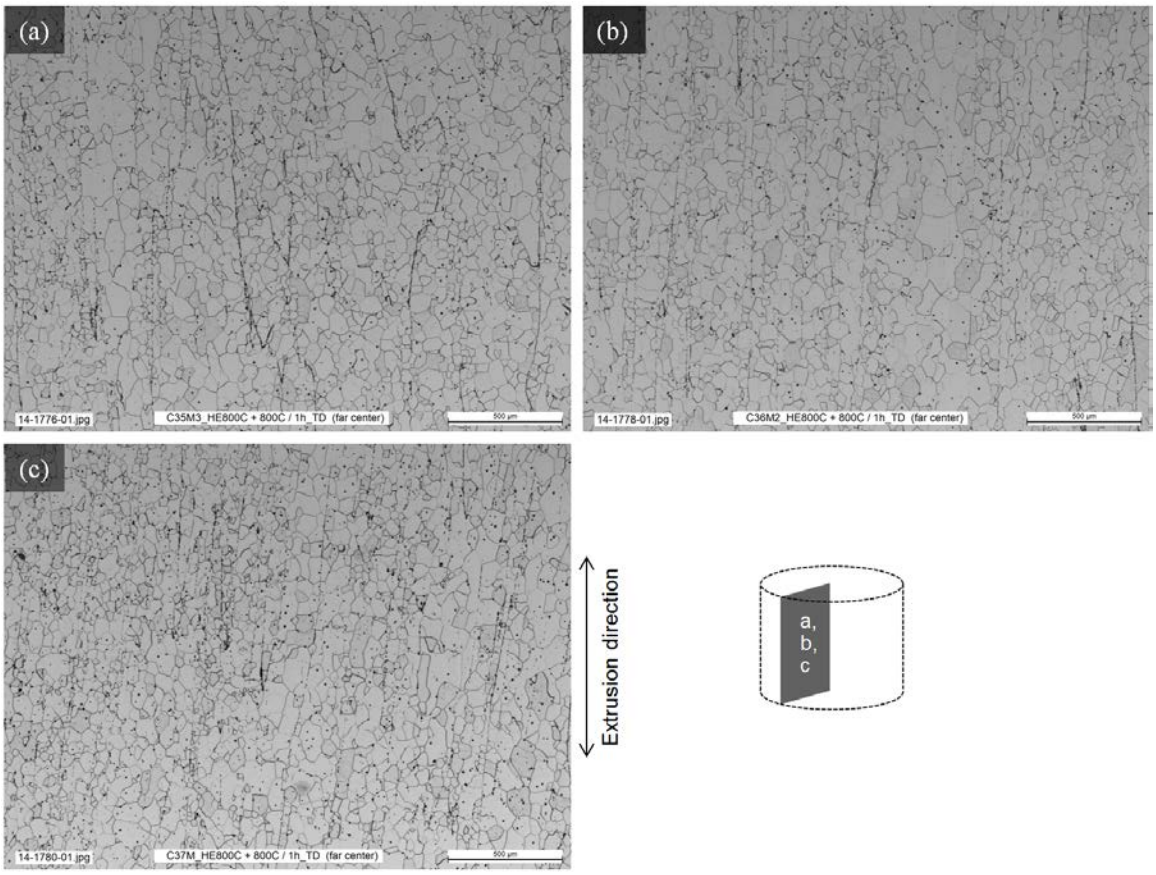

Figure 11. Optical micrographs showing microstructure of extruded and annealed C35M3, C36M2, and C37M; (a) as extruded, and (b) after annealing at 1100ºC for 10min

4.1.3. C06M2/C36M3

The as-received VIM ingots of the alloys C36M2 and C06M2 are shown in Figure 12. Both ingots show the crack formation at the "neck" below the hot-top similar to the C35MN6 ingots. However, the C06M2 (10Cr) alloy appeared to have reduced crack widths compared to C36M3 (13Cr), indicating that it may be somehow related to the Cr dependence of thermal expansion. The ingots were sectioned below the cracks, and then homogenized and machined similar to the other ingots discussed above.

There was no technical difficulty to conduct the hot-extrusion of the alloys C06M2 and C36M3 at 800ºC, as shown in Figure 13a. The extruded bars were straightened, annealed, and then machined to make bar specimens as shown in Figure 13b. They were provided to LANL for the parallel tube drawing study. No cracks or defects were observed in the machined bars.

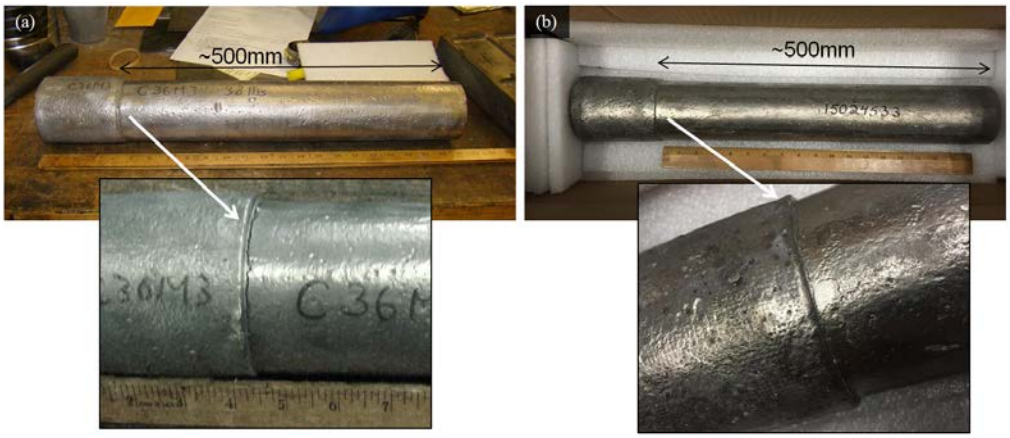

Figure 12. VIM ingots of C36M3 (a, 13Cr-6Al alloy) and C006M2 (b, 10Cr-6Al alloy) cast by Sophisticated Alloys, Inc.

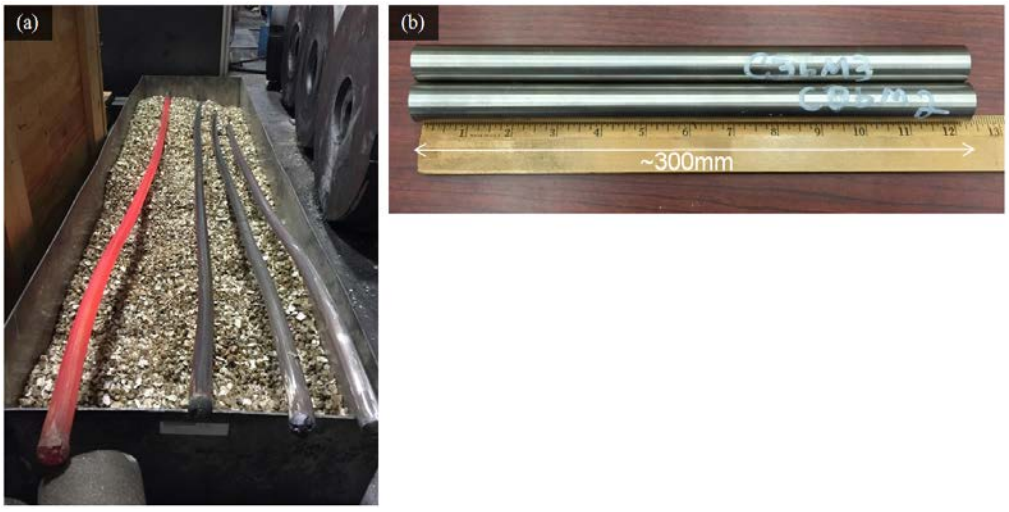

Figure 13. C36M3 and C06M2 extruded bars and master tubes to be tube-drawn; (a) as-extruded bars, and (c) master bars after surface grinding

4.2. Drawn tubes

In this section, the quality of the drawing process and the drawn tubes will be evaluated. Several issues were found which resulted in different types of failures during drawing processes, although most of the problems could be solved by optimization of the process conditions. The detailed failure characteristics of the tube drawing and the suggested solutions have been summarized below.

4.2.1. C35MN6

Figure 14 represents a typical problem of the C35MN6 master tubes observed after pointing, showing a crack in the upper tube formed along the longitudinal axis, but not in the lower tube. The pointing was conducted by a conventional swaging after soaking one end of the tubes at 1100ºC. Since this end did not show a visible crack before pointing, it was unclear why one tube showed the cracking and the other did not. One potential issue is that the stored energy might not be released by the annealing condition suggested in the Section 4.1.1., or the annealing process failed to achieve uniform temperature control or full recrystallization.

Figure 14. One end of C35MN6 master tubes after pointing, showing a crack along the longitudinal axis

Figure 15 illustrates the first trial tube drawing result of the C35MN6. The tube failed after the 3rd drawing pass with ~18% area reduction per pass (Figure 15a), and the ruptured surfaces aligned both longitudinal and transverse direction of the tube (Figure 15b). This result indicates that there might be two different failure modes: crack propagation along the longitudinal axis which might be attributed to the unleased stored energy in the deformed grains, similar to the crack formation at the pointing in Figure 14; or resistance of the tube deformation + the die

friction had exceeded the material strength which resulted in the necking and then fracture across the circumference direction. Figure 15c illustrates that another tube failed after the 1st drawing pass with 9-10% area reduction, and it showed a long crack along the drawing axis in the left-hand side, together with the ruptured surfaces with two failure modes similar to Figure 15b. It should be emphasized that one of the rupture surface along the drawing axis is almost on the same line of the long crack. This indicates that the crack initiation along the drawing axis could be correlated with pre-existing features (e.g. defects, deformed grains, etc.). It is also unclear why the second tube failed at the 1st drawing pass with lower area reduction than the first tube. However, it could be hypothesized that the tube conditions were not homogeneous from tube to tube or locations to locations. Four different tube drawing processes were attempted by changing the area reduction and the intermediate annealing temperatures, but none of them was successfully drawn to the target size of 9.5 mm OD and <0.4 mm wall thickness.

Figure 15. C35MN6 drawn tubes failed during drawing process; (a) after 3rd drawing pass with ~18% area reduction per pass, and (2) after 1st drawing pass with 9-10% area reduction

Figure 16 shows the cross-sectional microstructure of the drawn tubes compared to the as-extruded microstructure (the same picture shown in Figure 8a). Annealing at 1100ºC for 10 min

should be subjected to the master tubes prior to the drawing process, but the microstructure after drawing #1 (Figure 16b) was quite similar to the as-extruded one, indicating that the annealing condition was not sufficient to fully recrystallize the microstructure unlike the one shown in Figure 8b. The transverse section (Figure 16c) clearly indicated that the non-recrystallized grains showed further stain accumulation forming small cracks and potentially led to the large crack propagation inside such non-recrystallized grains.

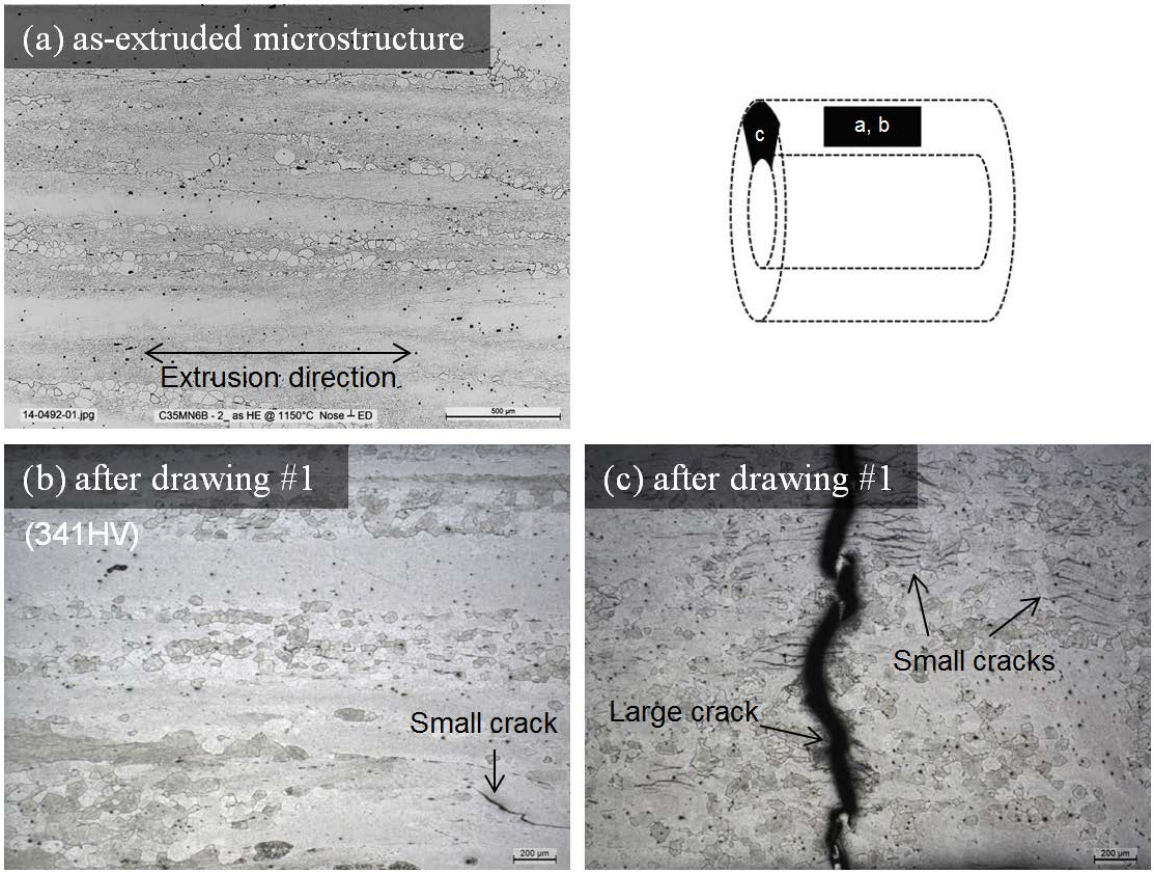

Figure 16. Optical micrographs of C35MN6 master and drawn tubes; (a) as-extruded tube, and (b,c) after 1st drawing with ~9-10% area reduction

Based on the results, it was concluded that there were several issues leading to the unsuccessful tube drawing of the alloy C35MN6 as listed below;

1. Tube extrusion might produce compressive stress accumulated the inner surface side of the tube wall along the circumference direction, which caused either a crack formation or the remained stored energy. In order to avoid such problem, a bar extrusion + gun-drilling would be preferable.
2. Insufficient annealing of the master tubes resulted in a non-optimized microstructure containing elongated, non-recrystallized coarse grains. This might have caused all observed failures of the alloy C35MN6 tube production. Uniform, fully recrystallized fine grain structure would be ideal to avoid unexpected crack propagation along the

elongated grains. Better temperature control of the annealing process as well as microstructure verification prior to the drawing process would be required.

3. Tube failure along transverse direction appears to be insensitive to the issues described above but is sensitive to drawing processing parameters such as the area of reduction (=deformation resistance during drawing) and the die friction. Grain refinement as well as alloy composition optimization should help to increase ductility or reduce the material strength. Intermediate annealing would also be important to control the deformability of the materials.

4.2.2. C35M3/C36M2/C37M

The second trial tube drawing was conducted with Nb-free Phase II alloys (C35M3) in order to avoid the observed issues above. The master tube was made by using the extruded bar + gun drilling process to minimize potential stored energy, and the refined grain structure could be easily obtained compared to the Nb containing alloys [6]. At the same time, the high Al containing alloys such as the alloys C36M2 and C37M were also selected to be drawn in order to see the effect of Al additions on the tube fabricability.

The results of the drawing process are summarized in Figure 17. There was no problem after the second drawing pass in all alloys. However, it was found that during the 3rd pass of the alloy C37M, the mandrel support inside the tube was broken leading to severe crack formation in the rest of the tube, as can be seen in Figure 17a. In the case of alloy C36M2, the tube ruptured three times during pointing before beginning the third pass, as shown in Figure 17b. Based on the results, the intermediate annealing was applied to the C35M3 after each drawing pass, and it resulted in making further tube-drawing of the C35M3 compared to the other alloys.

Several different intermediate annealing conditions were attempted over the course of the reduction process, and it caused the failure for some cases due to either insufficient recovery or over-annealing to reduce ductility. However, some parameters enabled successful fabrication of the thin-wall C35M3 tube with 9.5mm OD and <0.4mm WT, as shown in Figure 18. There were two tubes delivered with 400 mm and 520 mm length so far. A part of one tube was sectioned and used for the tube burst test specimen [13].

There were several quality issues found in the thin-wall C35M3 tubes. Figure 19 shows the cross-sectional microstructure of the as-received thin-wall C35M3 tube. It was found that the wall thickness was not uniform (Figure 19a) and they were in the range from 0.22 to 0.40 mm. Most of the grains showed irregular shape with the size more than 300 μm (Figure 19 b, c, and d) which were much coarser than the grains in the starting microstructure shown in Figure 11a. Since the number of the grains in the wall thickness seems only less than three at any locations, anisotropic deformation characteristics would easily be expected which should cause loss of concentricity of the tube wall during drawing process. The coarse grains also reduce the macroscopic ductility of the material, so that it may also cause premature failure during the drawing process.

Figure 17. Drawn tubes after several passes; (a) C37M failed after the 3rd drawing with ~9-11% area reduction per pass, (b) C36M2 failed after annealing and the 4th drawing, and (c) C35M3 with no failure after annealing and the 3rd drawing

Figure 18. C35M3 drawn tubes after several passes; (a) after further drawing, partially failed, and (b) as-received tubes with 9.5mm diameter and <0.40mm wall thickness, after final drawing and centerless grinding

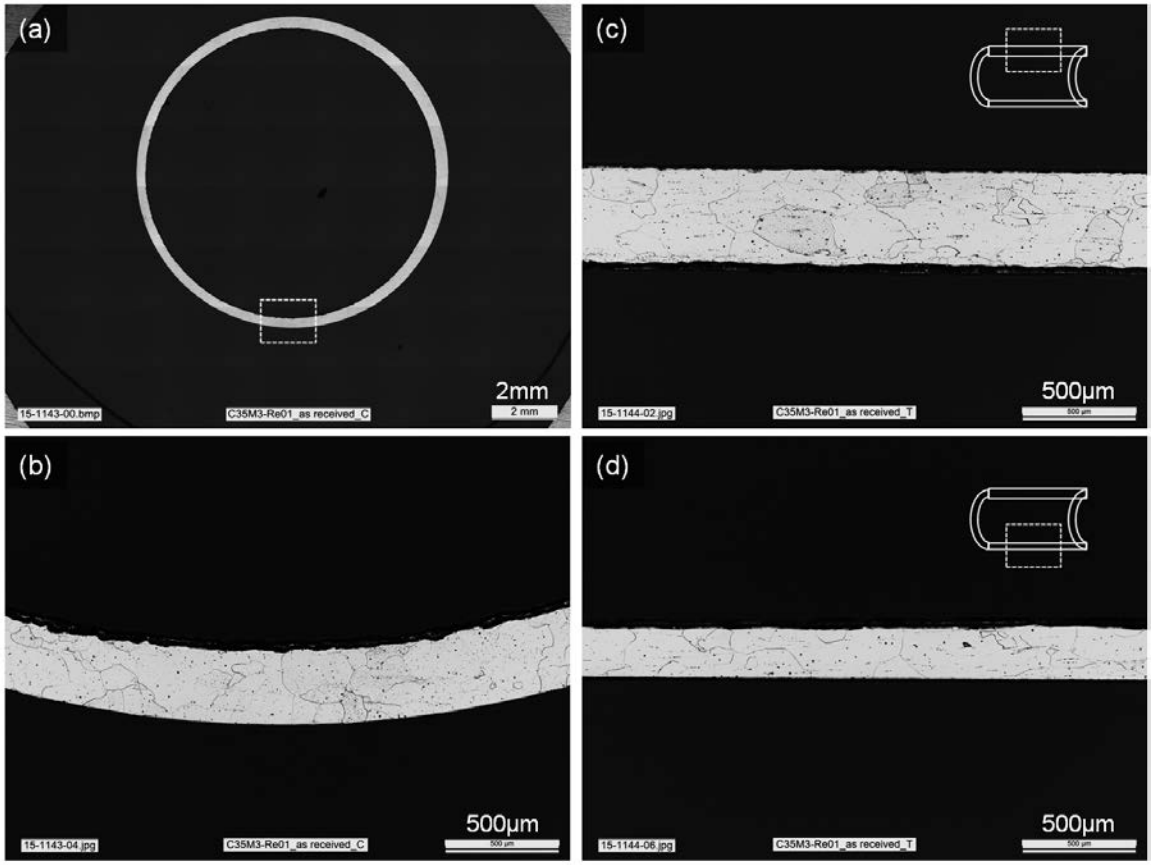

Figure 19. Cross-sectional optical micrographs of as-drawn C35M3; (a) an entire transverse section, (b) high magnification micrograph of a transverse section, (c) a longitudinal section of the thick-side wall, and (d) that of the thin-side wall

In order to understand the microstructure evolution of the alloy C35M3 during the drawing process, microstructural characterization of the tube after each drawing and annealing step was conducted. The tube drawing was performed at nominally 325ºC with ~9-11% thickness reduction per pass, and the intermediate annealing at 871ºC for 15-60 min was applied after every drawing step (other than the 1st drawing pass). Figure 20 depicts the microstructure evolution during drawing and annealing steps. Note that the detailed drawing parameters (e.g. OD, wall thickness, etc.) are not available. The as-drawn #2 specimen showed slightly elongated grains along the drawing direction, and the annealing resulted in eliminating such anisotropic features with a slight grain coarsening (the scale bars are different between Figure 20 a and b). Since a huge drop in hardness was observed after annealing, sufficient recovery took place to soften the material. After #6 drawing pass, the grain sizes seemed nearly doubled compared to the #2 drawn material with slightly elongated to the drawing direction. The total wall thickness reduction at this point was more than 50%, indicating that the annealing process after every drawing step resulted in spheroidizing the grains with minor coarsening. Short annealing times (15 min) resulted in irregular grain morphology and distribution of island-like coarsened grains as shown in Figure 20d, which seemed not ideal for the uniform deformation of the material. Actually, the tube was failed at the 7th drawing pass. It was also found that long annealing time

(60 min) also degraded the processbility, which could be due to the secondary recrystallization (grain coarsening), as can be seen in Figure 20f.

Figure 20. Cross-sectional optical micrographs of C35M3 during drawing steps; (a) after the 2nd drawing, (b) + annealing at 871ºC for 30min, (c) after the 6th drawing, (d) + annealing at 871ºC for 15min, (d) after the 13th drawing, and (e) + annealing at 871ºC for 60min

Figure 21a shows a picture of the failed C35M3 tubes. Detailed drawn parameters of each tube are not available, although from OD measurements, they failed at four different drawing steps. The rupture surfaces of all tubes were only through transverse direction, so that the issues #1 and #2 of the alloy C35MN6 discussed in Section 4.2.1 appeared irrelevant for this heat of material. Preliminary cross-sectional microstructure observation of the tube "B" with 14.1 mm OD (Figure 21b) indicated that the grain size is more than 100 µm which is much coarser than the initial microstructure shown in Figure 11a. The cross-sectional rupture surface revealed a heavy deformation with a necking feature, so that the failure should occur because the pulling load (= the deformation resistance at the die + the die friction) exceeded the ultimate tensile strength of the drawn tube. Since finer grain sizes promote better tensile properties at room temperature, refining grain size or preventing grain coarsening during drawing process could be a key for successful tube production.

Figure 21. (a) A picture showing C35M3 drawn tubes failed during drawing steps, and (b) a cross-sectional optical micrograph of the drawn tube "B" in the picture

Wall thickness distribution of the tubes in Figure 21a were measured and plotted in Figure 22. Four different wall thicknesses were measured as shown in the cartoon, and then compared with each other as a function of OD. The tube with the largest OD (the tube "B") showed thickest wall among the tubes, and the wall thickness decreased with decreasing the OD. The plot also clearly

indicated that the concentricity (or the uniformity of wall thickness) was gradually being lost as the drawing process progressed. It still requires the direct microstructure observation of each tube, but it can be easily speculated that the loss of concentricity is strongly correlated with the grain coarsening. Therefore, the grain refinement would also be a key for improving the quality of final tube products as well.

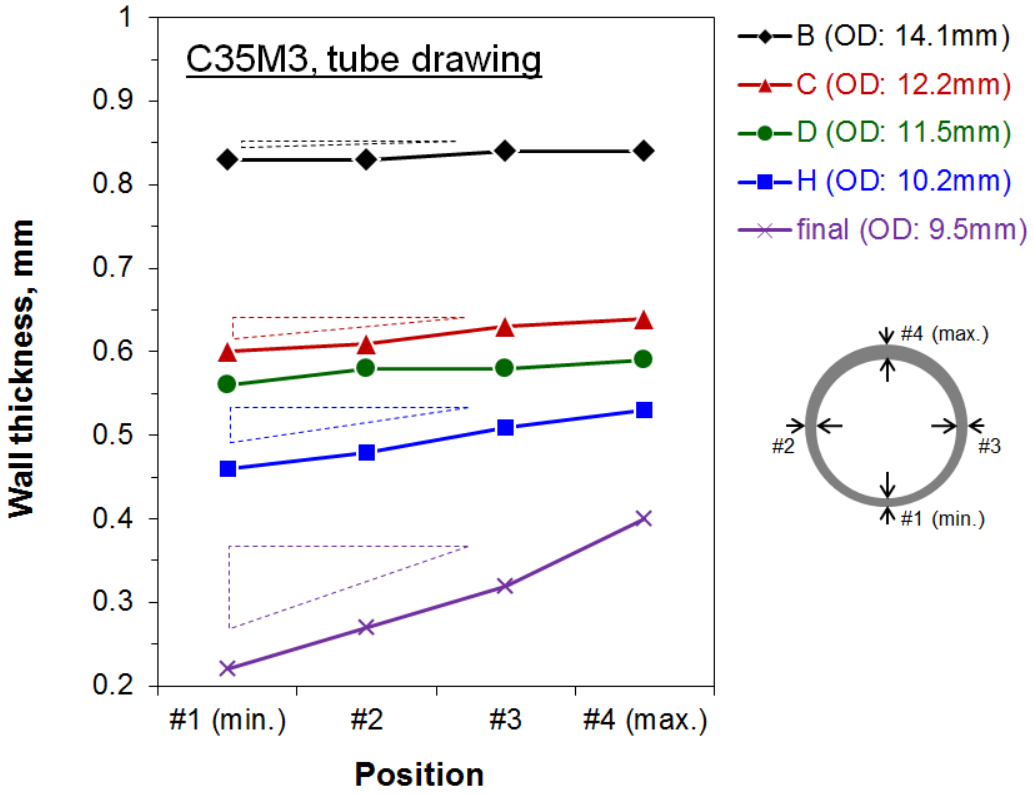

Figure 22. Wall thickness distribution of C35M3 drawn tubes showing that the concentricity decreases with proceeding the drawing process steps

In order to prevent the grain coarsening of the alloy C35M3 during tube drawing process, it is proposed to apply the intermediate annealing at lower temperature. It aims to have sufficient hardness drop to allow the further drawing but keep the deformed grain structure to eliminate any potential loss of concentricity. The optimization efforts are currently in progress.

4.2.3. Other tube fabrication processes

The compressive tube production route by using pilgering process would be easier to minimize the unexpected failures observed in the tube drawing process, since all alloys in this study were successfully rolled up to 93% thickness reduction with the following condition; (1) the initial microstructure should be uniform grain structure with sufficiently small grain size, such as ~50μm, and (2) the material should be soaked at 300ºC. The condition #1 can be easily achieved, but #2 may not be available, based on the discussion with STC and GE so far. Further discussion is planned.

5. SUMMARY AND CONCLUSIONS

This milestone report discusses the recent progress on the 2nd generation ATF FeCrAl cladding development involving commercial fabrication processes, in order to establish the industrial pathway for ATF FeCrAl thin-wall tube production, and to find potential issues to impact the quality of the final products. A warm tube-drawing process was selected for the initial tube production study, and the alloy Fe-13Cr-5.2Al-2Mo-1Nb-0.2Si-0.05Y (designation: C35MN6) was selected for the first tube production. The alloys Fe-13Cr-(5.2 or 6 or 7)Al-2Mo-0.2Si-0.05Y (C35M3, C36M2, and C37M, respectively) were used for the second trial. The alloys with Fe-(10 or 13)Cr-6Al-2Mo-0.2Si-0.05Y (C06M2 and C36M3, respectively) were also prepared and provided to Los Alamos National Laboratory (LANL) for the parallel effort of thin-wall tube production.

ATF FeCrAl tube-drawing production processes include alloy casting, master bar/tube production through extrusion and gun-drilling, and tube-drawing. The cast ingots are provided from Sophisticated Alloys, Inc. (SAI), Butler, PA. Small quantities of the cast ingots have been extruded at ORNL. Additionally, SAI will perform the extrusion once large quantity production is enacted (planned in FY2016). The gun-drilling and the tube drawing processes are conducted by Rhenium Alloys, Inc. (RAI), North Ridgeville, OH. LANL is currently working with Century Tubes, Inc., San Diego, CA, for the tube drawing processes. Superior Tube Company, Inc. (STC), Collegeville, PA, has a capability of High Precision Tube Roller (HPTR) cold-pilgering, and a discussion of trial pilgering processing of the 2nd generation ATF FeCrAl alloys are currently in progress among STC, General Electric (GE), and ORNL.

The first tube production with the alloy C35MN6 was unsuccessful. The ingot was tube-extruded at ORNL, and then annealed, machined, and then tube-drawn at RAI. The major failure was crack propagation along the extrusion/drawing axis which allows fewer than three drawing passes. It originated from a huge compressive stress accumulated at the inner surface side of the tube during the tube extrusion process, which resulted in either small crack formation or stored energy remaining in the tubes even without visible cracks. The annealing process prior to the drawing was found to be not sufficient to release stored energy, leaving the initial microstructure susceptible to crack initiation and propagation without further processing. Based on this failure and the evaluation of the process and microstructure, it was concluded that there were several issues to prevent the successful tube drawing of the alloy C35MN6 as listed below:

1. Tube extrusion might produce compressive stress accumulated at the inner surface of the tubes along the circumference direction, resulting in either crack formation or the remained stored energy. In order to avoid such problem, a bar extrusion + gun-drilling would be more preferable.
2. Insufficient annealing of the master tubes resulted in a non-optimized microstructure containing elongated, non-recrystallized coarse grains. This could be the primary mechanism for failures of alloy C35MN6 during tube production. Uniform, fully recrystallized fine grain structure would be ideal to avoid unexpected crack propagation along the elongated grains. Better temperature control of the annealing process as well as microstructure verification prior to the drawing process would be required.

3. Tube failure along the transverse direction appears to be insensitive to the issues described above but is sensitive to drawing processing parameters such as the cross-sectional area reduction (= deformation resistance during drawing) and the die friction. Grain refinement as well as optimized alloy composition should help to increase ductility or reduce the deformation resistance at the die. Intermediate annealing would also be important to control the deformability of the materials.

The second trial tube drawing was conducted with Nb-free Phase II alloys (C35M3) in order to avoid the observed issues in the alloy C35MN6. The master tube was made by using the extruded bar + gun drilling process to minimize potential stored energy. The refine grain structure could be easily obtained compared to the Nb containing alloys. The high Al containing alloys such as the alloys C36M2 and C37M were also selected to be drawn in order to see the effect of Al additions on the tube fabricability. The tube production of the alloys C36M2 and C37M was suspended after the failure during the third drawing pass, which could be due to the effect of the Al additions on increased work hardenability. The process of the alloy C35M3 continued, and after several attempts of different processing conditions, it had successfully been drawn into a thin-wall tube with 9.5 mm outer diameter and <0.40 mm wall thickness. However, two significant quality issues were found after the detailed inspections: firstly the wall thickness was not uniform; secondly that the grains had significantly coarsened. Microstructure characterization of the drawn tube at each step revealed that intermediate annealing applied for recovering the work hardening also caused significant grain coarsening, resulting in non-uniform deformability from locations to locations, and then losing concentricity of the drawn tube.

In order to prevent such grain coarsening of the alloy C35M3 during the tube drawing process, it is proposed to apply a lower temperature intermediate annealing. This recommendation aims to have sufficient hardness drop to allow for further drawing but keep the deformed grain structure to eliminate any potential loss of concentricity. Optimization efforts based on the recommendation are currently in progress.

6. REFERENCES

[1] Powers, D.; Meyer, R. Cladding swelling and rupture models for LOCA analysis, NUREG-0630; U. S. Nuclear Regulatory Commission: 1980.

[2] B. A. Pint, K. A. Unocic and K. A. Terrani, Materials at High Temperature, 32 (2015) 28-35.

[3] M. Moalem, D.R. Olander, Journal of Nuclear Materials 182 (1991) 170.

[4] K. Suzuki, S. Jitsukawa, N. Okubo, F. Takada, J.Nucl.Eng. and Design 240 (2010) 1290–1305.

[5] M. Steinbrück, M. Große, L. Sepold, J. Stuckert, Nuclear Engineering and Design 240 (7) (2010) 1714-1727.

[6] Y. Yamamoto, B.A. Pint, K. Terrani, K.G. Field, L.L. Snead, "Letter report documenting identifying billets and alloys fabricated for distribution to program" M3FT-13OR0202291, ORNL/LTR-2013/322, Oak Ridge National Laboratory (2013).

[7] P. Grobner, Metallurgical and Materials Transactions B, 4 (1973) 251-260.

[8] K.G. Field, X. Hu, K.C. Littrell, Y. Yamamoto, L.L. Snead, "Radiation Tolerance of Neutron-Irradiated Model Fe-Cr-Al Alloys," Journal of Nuclear Materials, 465 (2015) 746-755.

[9] K.G. Field, M.N. Gussev, Y. Yamamoto, L.L. Snead, "Deformation behavior of laser welds in high temperature oxidation resistant Fe-Cr-Al alloys for fuel cladding applications," Journal of Nuclear Materials, 454 (2014) 352-358.

[10] B. A. Pint, S. Dryepondt, K. A. Unocic, and D. T. Hoelzer, JOM, 66 (2014) 2458-2466

[11] H. Qu, Y. Lang, C. Yao, H. Chen, C. Yang, Materials Science and Engineering: A 562 (2013) 9-16.

[12] Y. Yamamoto, Y. Yang, K.G. Field, K. Terrani, B.A. Pint, and L.L. Snead, "Letter Report Documenting Progress of Second Generation ATF FeCrAl Alloy Fabrication, FY14 FCRD milestone report," M3FT-14OR0202232, ORNL/LTR-2014/219, Oak Ridge National Laboratory (2014).

[13] Y. Yamamoto, M.N. Gussev, B.K. Kim, T.S. Byun, "Optimized properties on base metal and thin-walled tube of Generation II ATF FeCrAl", M2FT-15OR0202291, ORNL/TM-2015/414 (2015).

[14] B.A. Pint, K.A. Unocic, K.A. Terrani, "Steam Oxidation of FeCrAl and SiC in the SATS", M3FT-15OR0202342, ORNL/LTR-2015/417 (2015).

[15] "Shanghai EverSkill M&E Co., Ltd": *http://www.esmeind.com/Pro-Tube.html#*

[16] "Cold Pilger Rolling: Part One" in the website of Total Materia, Apr. 2013: *http://www.totalmateria.com/page.aspx?ID=CheckArticle&site=kts&NM=396*

[17] Albert Nerino, Mark Deaver, Chris Nagele, John Reinhart , "HPTR's past, present, and future — Part I", TPJ - THE TUBE & PIPE JOURNAL®, Jun. 2011: *http://www.thefabricator.com/article/tubepipeproduction/hptras-past-present-and-future-a-part-i*